Available online at www.sciencedirect.com
ScienceDirect
Surface & Coatings Technology 201 (2007) 8830–8837
SURFACE & COATINGS TECHNOLOGY
www.elsevier.com/locate/surfcoat

Modeling multiscale effects on transients during chemical vapor deposition

Matthias K. Gobbert [a,*], Timothy S. Cale [b]

[a] Department of Mathematics and Statistics, University of Maryland, Baltimore County, 1000 Hilltop Circle, Baltimore, MD 21250, U.S.A.
[b] Department of Chemical and Biological Engineering, Rensselaer Polytechnic Institute, Ri 131, 110 8th Street, Troy, NY 12180-3590, U.S.A.

Available online 10 May 2007

Abstract

Several important manufacturing processes for integrated circuits (ICs) involve the flow of gaseous reactants over the wafer(s) on which the ICs are being made. We discuss a model in which reactive components of the gas phase do not collide; either because there is a dominant carrier species, or the pressure is low enough. The kinetic transport and reaction model consists of a system of transient linear Boltzmann equations for the reactive species in the flow. This model applies to a wide range of transport regimes, characterized by a wide range of Knudsen numbers as a function of pressure and length scale of interest. A numerical simulator based on a spectral Galerkin method in velocity space approximates each linear Boltzmann equation by a system of transient conservation laws in space and time with diagonal coefficient matrices, which are solved using the discontinuous Galerkin method. This deterministic solver gives direct access to the kinetic density that is the solution to the Boltzmann equation, as a function of position, velocity, and time. The availability of the kinetic density as a function of velocity is useful to analyze the underlying kinetic causes of macroscopic observables. Using chemical vapor deposition as an important application example, the influence of process parameters is studied in transient two-dimensional and three-dimensional features that represent structures seen during integrated circuit fabrication for a wide range of Knudsen numbers. The results highlight the capabilities of the KTRM and its implementation, and indicate that kinetic solvers may be needed for models characterized by Knudsen numbers on the order of unity. This regime applies both to feature scale simulators at certain operating conditions and to intermediate scale models used as part of multiscale simulators.

Keywords: Multiscale modeling; Kinetic transport and reaction modeling; Chemical vapor deposition; Deterministic numerical method

1. Introduction

Multiscale modeling of chemical vapor deposition (CVD) and other microelectronics manufacturing processes is particularly challenging when different types of models are appropriate on different length scales [1]. The dimensionless group that characterizes the applicability of the different models is the Knudsen number Kn; it is the ratio of the mean free path to a characteristic length scale of the domain of interest. For $Kn \ll 1$, typical of the reactor scale, continuum transport and reaction models are used [2,3]. For $Kn \gg 1$, typical of the feature scale, free molecular or ballistic transport and reaction models are used [4]. Approaches to models in the intermediate regime with $Kn \approx 1$ need to take collisions into account and result in integral equations or integro-differential equations such as the Boltzmann Transport Equation (BTE) [1,5,6] The numerical techniques appropriate for use with continuum and kinetic models are different. In turn, the codes that solve each type of model need to be interfaced for a fully integrated model of the process.

Early approaches to combining reactor scale and feature scale models used a top-down approach that fed information from the decimeter to the micrometer scale [7,8]. A fully integrated multiscale model provides concurrent solution of models for all relevant scales and provides information flow both upscale and downscale. To develop an integrated, deterministic, multiscale CVD model, we introduced a mesoscopic scale model; i.e., a model on the millimeter length scale. This type of model covers the length scale of several feature clusters, each perhaps containing thousands of features. It is useful in studying cluster-to-cluster effects [9], and it provides an interface between models and simulators on the reactor and feature scales. In this spirit, we presented a fully integrated three-scale CVD simulator in [10,11]. In this three-scale

* Corresponding author.
E-mail address: gobbert@math.umbc.edu (M.K. Gobbert).

0257-8972/$ - see front matter © 2007 Elsevier B.V. All rights reserved.
doi:10.1016/j.surfcoat.2007.05.005

approach, continuum models were used for both the reactor scale and the mesoscopic scale and were solved using FIDAP [12]. The Ballistic Transport and Reaction Model (BTRM) was used for the feature scale, and was solved using EVOLVE [13].

Our desire to study transients and to extend transport and reaction modeling into the transition transport regime, where $Kn \approx 1$, motivated the development of an explicitly kinetic or BTE based approach. We introduced the Kinetic Transport and Reaction Model (KTRM), with a focus on transients during atomic layer deposition (ALD) in [14–17]. That work treated $Kn \gg 1$, in which the collision terms of the BTE can be neglected.

We provided a formal derivation of the multi-species KTRM valid for the full range of Knudsen numbers in [18]. The goal of that work was to lay the rigorous foundation for using the KTRM as part of a multiscale model. We studied CVD on the feature scale, for Kn values from $\ll 1$ to ∞ by varying (formally) the pressure in the model in the context of a relevant application. Equally important, the numerical simulator used to solve the KTRM was tested for a range of Kn, from small to large, and its reliability was discussed in [19]. Note that in collisional systems, the KTRM is valid for cases in which there is a dominant background species; e.g., a carrier gas [18].

Other work has focused on extending the simulator and its applicability specifically to three-dimensional models with features of more realistic complexity that require a general three-dimensional mesh without symmetries [20], such as a trench with a central via below the trench shown in Fig. 1 (a). We have also started to analyze the behavior of the KTRM and its simulator on different time scales as a function of the Knudsen number [21]. This work is continued in the present paper for a representative two-dimensional trench shown in Fig. 1 (b). The results demonstrate that lower Kn lead to longer transients. However, since the kinetic densities quickly reach the shape of Maxwellians, macroscopic observables are indeed sufficient to model these cases. This shows that traditional continuum-based models and their simulations are appropriate for small Kn. The explicit access to the kinetic density $f(\mathbf{x}, \mathbf{v}, t)$ as a function of $\mathbf{v}$ afforded by a deterministic numerical method for a kinetic model allows us to analyze the underlying dependence of f on velocity components to justify this conclusion. For cases of moderate to large Kn though, the kinetic density never assumes the shape of a Maxwellian and it is advantageous to have access to $f(\mathbf{x}, \mathbf{v}, t)$ as function of all its variables to analyze the behavior of the model, justifying the added computational effort required. These conclusions apply particularly for intermediate $Kn \approx 1$, which is the expected regime for intermediate scale models as part of a multiscale simulator.

Section 2 provides a brief overview of the KTRM. Section 3 summarizes the numerical method. Sections 4.1 and 4.2 present the simulation results for the domains in Fig. 1 (b) and (a), respectively. The results are discussed in Section 5.

2. The model

Gas flow in the desired regimes, particularly for both collisionless transport ($Kn \gg 1$) and transport in the transition regime ($Kn \approx 1$), is appropriately modeled by the Boltzmann transport equation (BTE). For $Kn \ll 1$, traditional continuum approaches are more appropriate in practice because of their numerical efficiency. For a multi-species model, we have the system of dimensional non-linear Boltzmann transport equations for all gaseous species (including the carrier gas with species label $i=0$) [5,6,18]

$$\frac{\partial f^{(i)}}{\partial t} + \mathbf{v}\cdot\nabla_{\mathbf{x}} f^{(i)} = \sum_{j=0}^{n_s} Q_{ij}\left(f^{(i)}, f^{(j)}\right), \quad i = 0, 1, \ldots, n_s, \qquad (1)$$

where the left-hand side models the transport of species i and the right-hand side models all interactions (collisions and reactions) of species i with all other species $j=0, 1,\ldots, n_s$ through the non-linear collision operators $Q_{ij}(f^{(i)}, f^{(j)})(\mathbf{x}, \mathbf{v}, t)$.

The unknown functions $f^{(i)}(\mathbf{x}, \mathbf{v}, t)$ in this kinetic model represent the (scaled) probability density, called the kinetic density in the following, that a molecule of species $i=0, 1,\ldots, n_s$ at position $\mathbf{x} \in \Omega \subset \mathbb{R}^3$ has velocity $\mathbf{v} \in \mathbb{R}^3$ at time t. We present the

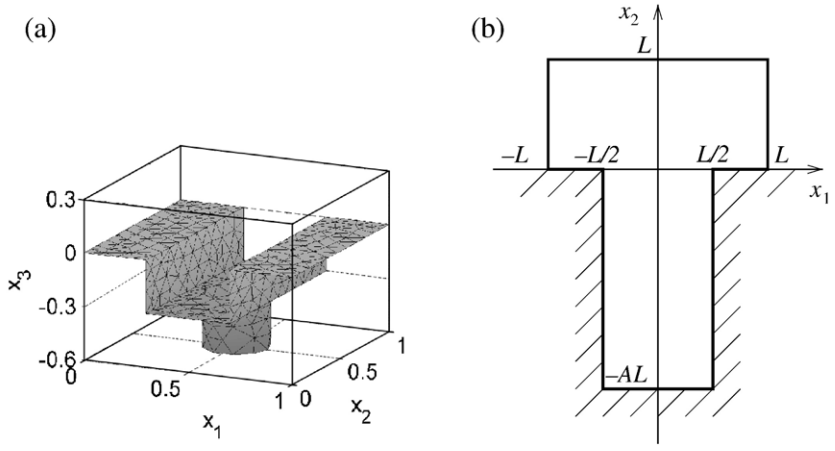

Fig. 1. Schematics of (a) a three-dimensional trench-via structure (known as a 'Damascene' structure in industry) and (b) a two-dimensional trench defining the feature width L and aspect ratio A. Each plot shows the solid wafer surface. The gas domain of the KTRM is the region above the wafer surface up to the top of the plot box.

model equations here and in the following section in three-dimensional notation for definiteness, but both models in two and three dimensions are useful in practice and will be considered in Section 4. The values of the kinetic densities need to be determined at all points $\mathbf{x}$ in the three-dimensional spatial domain Ω and for all three-dimensional velocity vectors $\mathbf{v}$ at all times $0<t\le t_{\text{fin}}$. This high dimensionality of the space of independent variables is responsible for the numerical complexity of kinetic models, as six dimensions need to be discretized, at every time step for transient simulations.

The system of partial differential equations in (1) is coupled to boundary conditions at the surface of the domain $\Omega\subset\mathbb{R}^3$. At the top of the domain is the interface to the bulk domain of the chemical reactor, and the flow is modeled as a Maxwellian distribution there. The crucial boundary condition for applications in microelectronics manufacturing is along the wafer surface Γ_w at the bottom of the domain for all reactive species $i=1,\ldots,n_s$ [18]

$$f^{(i)}(\mathbf{x},\mathbf{v},t)=C_i[\eta_i(\mathbf{x},t)+r_i(\mathbf{x},t)]M^{(i)}(\mathbf{v}),\quad \mathbf{x}\in\Gamma_w\quad \mathbf{n}\cdot\mathbf{v}<0. \tag{2}$$

This condition models the inflow components of the kinetic density ($\mathbf{n}\cdot\mathbf{v}<0$ with outward unit normal vector $\mathbf{n}(\mathbf{x})$ at $\mathbf{x}\in\Gamma_w$) as a re-emission of molecules from the wafer with a velocity distribution of Maxwellian shape and proportional to the outward flux $\eta_i(\mathbf{x},\ t)$ plus the species generation rate $r_i(\mathbf{x},\ t)$ of any molecules created in or re-emitted by surface reactions. The scaling factor C_i is chosen to ensure mass conservation in the case that all molecules re-emit from the surface. This boundary condition connects to the surface reactions only through the species generation rate $r_i(\mathbf{x},\ t)$ of the reactive gaseous species, and thus it allows for the use of any general, non-linear reaction model at the surface, involving potentially other surface species in addition to the gaseous species. Examples of a two-species model with two surface reactions were developed for the reaction step of ALD in [15–17].

The dimensional model in (1) involves a carrier species that is assumed to be dominant and inert, denoted by $i=0$. Using these assumptions, a generalizations of assumptions in [5], the equation for the inert carrier gas decouples from all other equations and we can obtain a model for the reactive species only. Moreover, collisions of each reactive species with the carrier species are the dominant effect in the gas phase of the model on this scale. Therefore, we obtain a system of linear Boltzmann equations for the KTRM that only involves the reactive gaseous species $i=1,\ldots,n_s$ and the linear collision operators $Q_i(f^{(i)})(\mathbf{x},\mathbf{v},t)$ [18], reading in dimensionless form

$$\frac{\partial f^{(i)}}{\partial t}+\mathbf{v}\cdot\nabla_{\mathbf{x}}f^{(i)}=\frac{1}{Kn}Q_i\left(f^{(i)}\right),\quad i=1,\ldots,n_s, \tag{3}$$

with the linear collision operators

$$Q_i\left(f^{(i)}\right)(\mathbf{x},\mathbf{v},t)=\int_{\mathbb{R}^3}\sigma_i(\mathbf{v},\mathbf{v}')\left[M^{(i)}(\mathbf{v})f^{(i)}(\mathbf{x},\mathbf{v}',t)-M^{(i)}(\mathbf{v}')f^{(i)}(\mathbf{x},\mathbf{v},t)\right]d\mathbf{v}', \tag{4}$$

where $\sigma_i(\mathbf{v},\ \mathbf{v}')=\sigma_i(\mathbf{v}',\ \mathbf{v})\ge 0$ is a given collision frequency model and $M^{(i)}(\mathbf{v})$ denotes the Maxwellian distribution of species i. This model together with the boundary conditions (2) only involve the reactive species $i=1,\ldots,\ n_s$. It is non-dimensionalized by scaling the transport on the left-hand side with respect to the typical domain size L^*, while the collision operator on the right-hand side is non-dimensionalized with respect to the mean free path of the mixture λ. Thus, the Knudsen number $Kn=\lambda/L^*$ arises formally as the dimensionless group in (3). The values of Kn are affected by both the scale of interest of the model and by the mean free path through the operating conditions of the chemical reactor. Notice that while the partial differential equations in (3) are decoupled, the model couples all reactive species through the boundary conditions at the wafer surface (2) that connects to the surface reaction model and is of crucial importance for the applications under consideration.

3. The numerical method

The numerical method for (3)–(4) needs to discretize the spatial domain $\Omega\subset\mathbb{R}^3$ and the (unbounded) velocity space $\mathbb{R}^3$. We start by approximating each $f^{(i)}(\mathbf{x},\ \mathbf{v},\ t)$ by an expansion $f_K^{(i)}(\mathbf{x},\mathbf{v},t):=\sum_{\ell=0}^{K-1}f_\ell^{(i)}(\mathbf{x},t)\varphi_\ell(\mathbf{v})$. Here, the basis functions $\varphi_\ell(\mathbf{v})$ in velocity space are chosen such that they form an orthogonal family of functions in velocity space with respect to a weighted L^2-inner product.

Inserting the expansion for $f^{(i)}(\mathbf{x},\ \mathbf{v},\ t)$ and testing successively against $\varphi_k\ (\mathbf{v})$ with respect to the inner product approximates (3) by a system of linear hyperbolic equations [19]

$$\frac{\partial F^{(i)}}{\partial t}+A^{(1)}\frac{\partial F^{(i)}}{\partial x_1}+A^{(2)}\frac{\partial F^{(i)}}{\partial x_2}+A^{(3)}\frac{\partial F^{(i)}}{\partial x_3}=\frac{1}{Kn}B^{(i)}F^{(i)},\quad i=1,\ldots,n_s, \tag{5}$$

where $F^{(i)}(\mathbf{x},t):=\left(f_0^{(i)}(\mathbf{x},t),\ldots,f_{K-1}^{(i)}(\mathbf{x},t)\right)^T$ is the vector of the K coefficient functions in the expansion in velocity space. Here, $A^{(1)}$, $A^{(2)}$, $A^{(3)}$, and $\mathrm{B}^{(i)}$ are constant $K\times K$ matrices.

Using collocation basis functions, the coefficient matrices $A^{(1)}$, $A^{(2)}$, $A^{(3)}$ become diagonal matrices [19]. Note again that the equations for all species remain coupled through the crucial reaction boundary condition at the wafer surface.

The hyperbolic system (5) is now posed in a standard form as a system of partial differential equations on the spatial domain Ω and in time t and amenable to solution by various methods. Since typical domains in our applications such as shown in Fig. 1 (a) are of irregular shape, we use the discontinuous Galerkin method (DGM) [22], relying on a finite element discretization of the domain Ω.

The implementation of the numerical method permits for switching between various triangular and quadrilateral meshes in two and three dimensions and provides an effective parallel implementation. The degrees of freedom (DOF) of the finite element method are the values of the n_s species' coefficient functions $f^{(i)}(\mathbf{x},\ t)$ in the Galerkin expansion at K discrete velocities on the vertices of each of the N_e elements of the finite

element mesh. In two dimensions, we use a 8×8 velocity mesh in $\mathbb{R}^2$ and a spatial mesh of the trench in Fig. 1 (b) with $N_e=80$ quadrilateral elements, thus the number of DOFs are (4)(64)(80)=20,480 at every time step. In three dimensions, we use a $4\times4\times4$ velocity mesh in $\mathbb{R}^3$ and a spatial mesh of the trench-via structure in Fig. 1 (a) with $N_e=7{,}087$ tetrahedral elements,

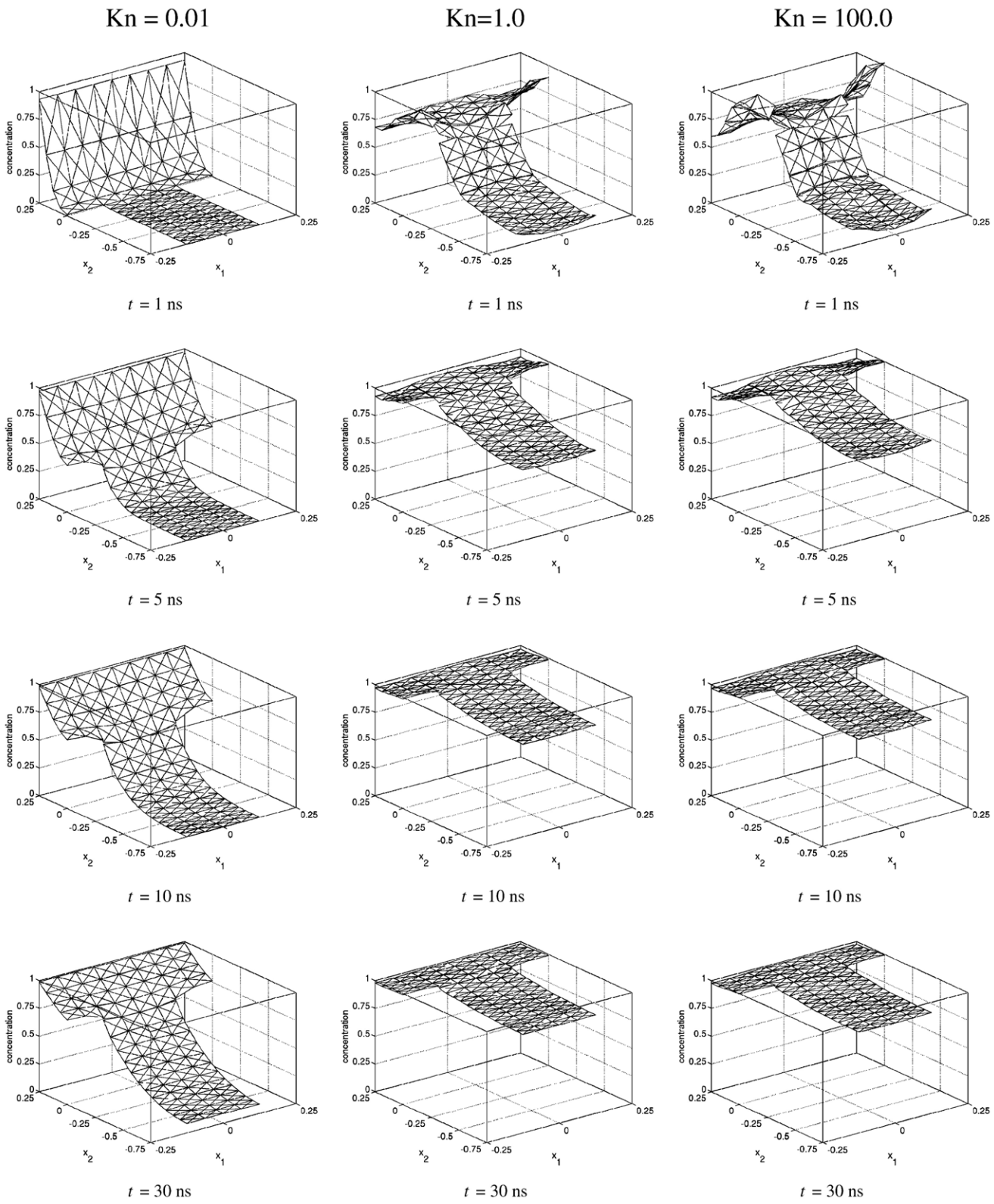

Fig. 2. Dimensionless concentration $c(\mathbf{x}, t)$, as a function of $\mathbf{x}$ in the two-dimensional trench for selected Kn at selected times. The vertical scale ranges from 0 to 1 in all plots.

hence the number of DOFs are (4)(64)(7087)=1,814,272 at every time step. Extensive validations of the numerical method and convergence studies for a wide range of Knudsen numbers are the focus of [19].

4. Results

In order to focus on the transients, we consider a simple, linear (constant sticking factor) CVD chemistry with one reactant species

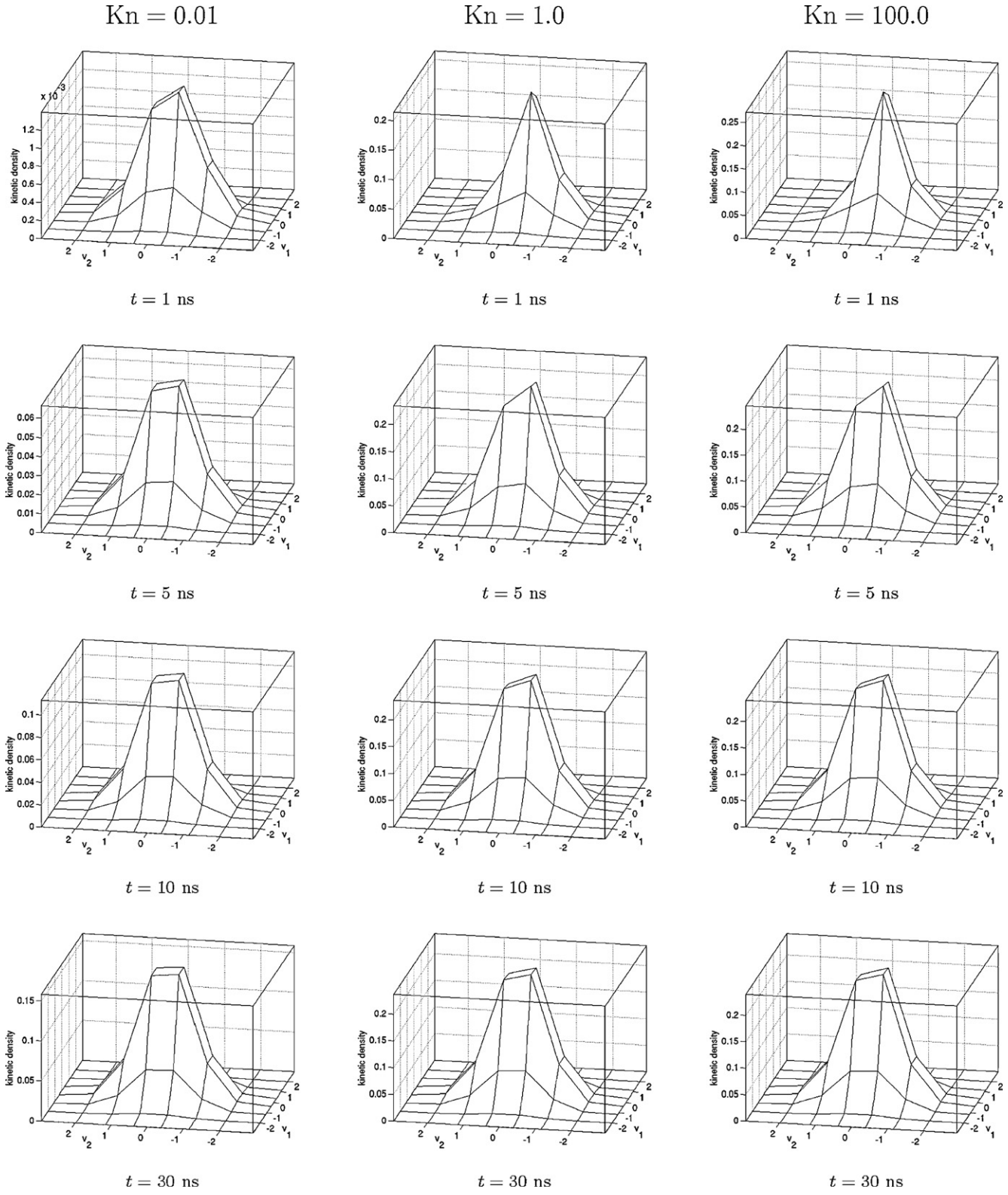

Fig. 3. Dimensionless kinetic density $f(\mathbf{x}, \mathbf{v}, t)$ as a function of $\mathbf{v} \in \mathbb{R}^2$ at $\mathbf{x}=(0.0625, 0.0)$ in the two-dimensional trench for selected *Kn* at selected times. Notice the different scales on the vertical axes in some plots.

(n_s=1); in the following, we drop the species index i=1 in this single-species model. The following results show simulations for both domains shown in Fig. 1. The reactant is supplied from the gas-phase interface at the top of the domain and deposits at the wafer surface with a sticking factor of γ=0.01 [3]. For the reactive gaseous species, this gives a species generation rate of $r(\mathbf{x}, t)=-\gamma\eta(\mathbf{x}, t)$ and thus the boundary condition (2) becomes $f=C\,[1-\gamma]\,\eta\,M$. The collision operator uses a relaxation time

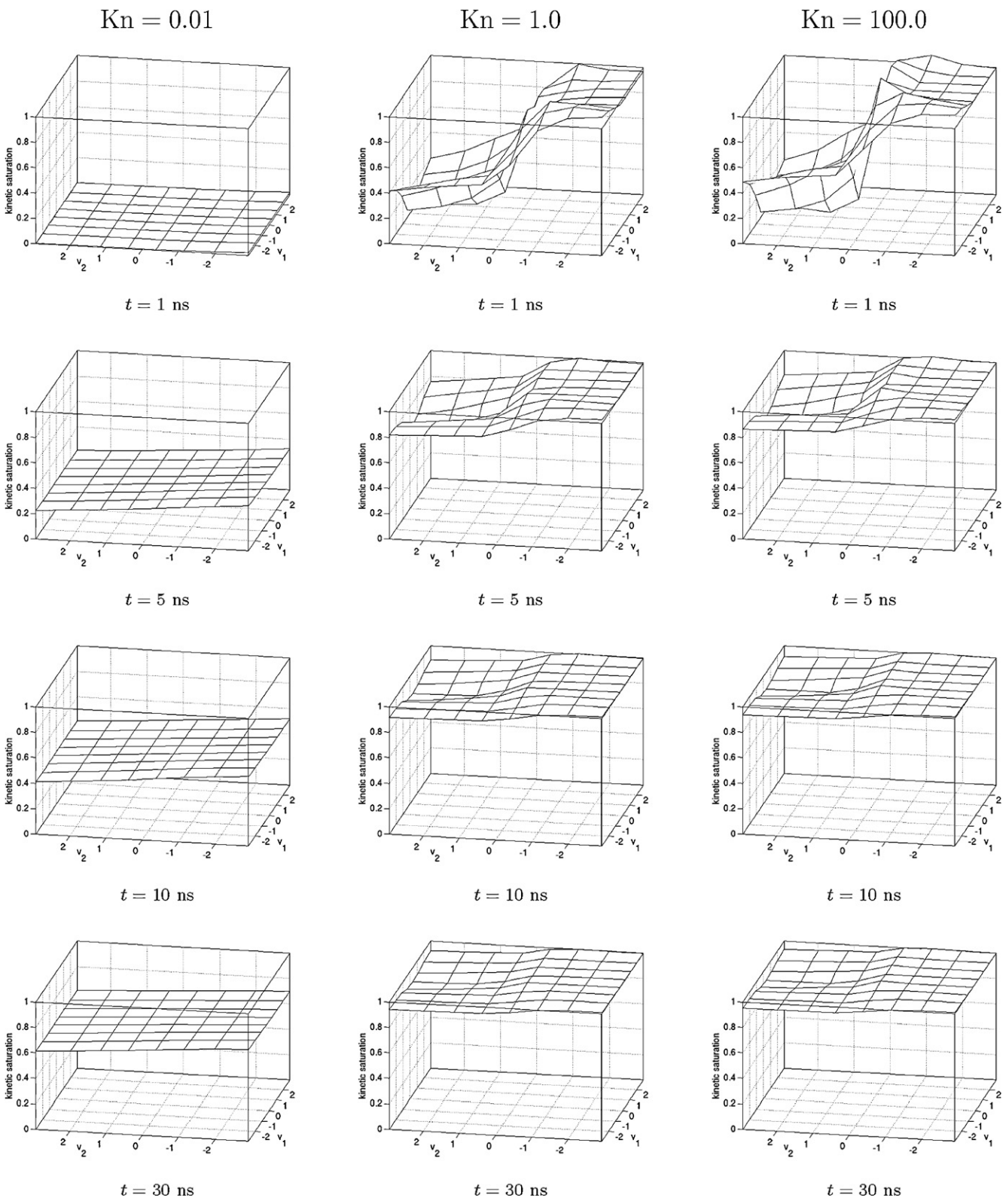

Fig. 4. Saturation of kinetic density $f(\mathbf{x}, \mathbf{v}, t)/M(\mathbf{v})$ as a function of $\mathbf{v}\in\mathbb{R}^2$ at $\mathbf{x}$=(0.0625, 0.0) in the two-dimensional trench for selected *Kn* at selected times. The vertical scale ranges from 0 to 1 in all plots.

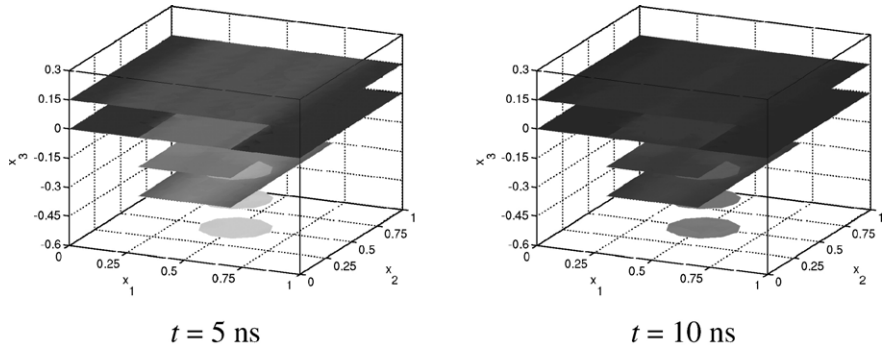

Fig. 5. Slice plots of the dimensionless concentration $c(\mathbf{x}, t)$ for $Kn=1.0$ at heights $x_3=-0.60, -0.45, -0.30, -0.15, 0.00, 0.15$ at different times. Grayscale from light $\Leftrightarrow c=0$ to dark $\Leftrightarrow c=1$.

approximation by choosing $\sigma(\mathbf{v}, \mathbf{v}')\equiv 1/\tau$ in (4) with (dimensionless) relaxation time $\tau=1.0$ that characterizes the time to return to steady-state under appropriate boundary conditions. The temperature in this micron-scale domain is assumed constant and uniform throughout the domain and is set at $T=500$ K [18]. We focus on how the flow behaves when starting from no reactive gas present, as modeled by initial condition $f\equiv 0$ at $t=0$ for the reactive species; the inert species is already present throughout the domain [18].

4.1. Two-dimensional trench

Figs. 2, 3 and 4 show simulation results for the two-dimensional trench of Fig. 1 (b). The trench is modeled as 0.25 μm wide with aspect ratio 3. The reactive species is fed at the top of the domain at $x_2=0.25$ μm.

Fig. 2 shows the dimensionless concentration $c(\mathbf{x},t) := \int\!\!\int f(\mathbf{x},\mathbf{v},t)d\mathbf{v}$ vs. $\mathbf{x}=(x_1, x_2)$. The columns show the transient results at selected (re-dimensionalized) times for $Kn=0.01$, 1.0, and 100.0, as specified at the top of the figure. The vertical scale ranges from 0 to 1 in all plots. Starting from $c=0$ at $t=0$ (not shown), the concentration increases from the source at the top of the domain, as seen in the first row of plots for $t=1$ ns. From there on, the concentration increases faster in the cases of larger Kn, because the flow tends to be more directional. For $Kn<1$, the collisions tend be more dominant and thus the concentration profiles smoother, but it takes longer for significant numbers of molecules to reach the feature bottom at $x_2=-0.75$ μm.

The key advantage of the KTRM is that we have direct access to the kinetic density $f(\mathbf{x}, \mathbf{v}, t)$ as a function of velocity $\mathbf{v}$. This is demonstrated by Fig. 3, whose plots show $f(\mathbf{x}, \mathbf{v}, t)$ vs. $\mathbf{v}=(v_1, v_2)\in\mathbb{R}^2$ at the position $\mathbf{x}=(x_1, x_2)=(0.0625, 0.0)$ at the feature mouth for the same times and Kn as Fig. 2. Notice that the vertical scales are different in some of the plots. The v_1–v_2-axes are slightly rotated so that the v_2 is at the front of the plot with negative values on the right; this means that velocity directions pointing downward into the trench are in the right half of each plot. We see that the shape of f tends to a Maxwellian for $Kn=0.01$, but notice that its maximum has not yet reached the height of the Maxwellian at steady-state. By contrast, the kinetic density for the larger values of Kn has a larger maximum value much faster, but the shape remains noticeably unsymmetrical, indicating that the flow direction remains downward.

Because the numerical values of the components of f vary widely in size, it is useful to define the saturation $f(\mathbf{x}, \mathbf{v}, t)/M(\mathbf{v})$. This is plotted vs. $\mathbf{v}\in\mathbb{R}^2$ in Fig. 4. The horizontal v_1–v_2-axes are rotated as in Fig. 3. The vertical scale ranges from 0 to 1 in all plots. We can readily see the smoother shape of f for the smaller Kn. Particularly for $Kn=100.0$, it is visible that there are very few upward velocity components at $t=1$ ns. These components only arise later as molecules return from re-emission at the wafer surface.

4.2. Three-dimensional trench-via structure

Figs. 5 and 6 show representative simulation results for the three-dimensional trench-via structure of Fig. 1 (a). The reactive species is fed at the top at $x_3=0.3$ μm.

Fig. 5 shows slice plots of the concentration $c(\mathbf{x}, t)$ as a function of $\mathbf{x}=(x_1, x_2, x_3)$ for the example of the Knudsen number $Kn=1$ in the transition regime. The shapes of the slices indicate the shape of the domain Ω of Fig. 1 (a). The values of c are indicated by the gray scale. We can see that at $t=5$ ns the mean wafer surface at $x_3=0.0$ has already been saturated, but not the bottom of the via at $x_3=-0.6$. By $t=10$ ns, substantially more molecules have reached the bottom of the via.

To analyze the directionality of the flow, one can consider the kinetic density $f(\mathbf{x}, \mathbf{v}, t)$ as a function of $\mathbf{v}=(v_1, v_2, v_3)$ at selected points $\mathbf{x}=(x_1, x_2, x_3)$. We select the two points (0.5, 0.5, 0.0) and (0.5, 0.5, −0.3); both lie in the central axis of the via with $x_1=x_2=0.5$; the first point with $x_3=0.0$ is at the height of the trench mouth, while the second one with $x_3=-0.3$ is at the via mouth. As before, to show more clearly the effect also on the components of f with smaller numerical values, we plot the saturation of the kinetic density f/M. At the point $\mathbf{x}$ in the center of the domain, f is symmetric with respect to the v_1 and v_2 components, hence we fix $v_1=v_2=0$ here and consider f/M as a function of v_3 only. This leads to the plots in Fig. 6. Starting from the initial condition $f=0$, the saturation increases over time in all components. At first, the increase is in the downward components (in the left half of the plot), then also in the upward components (right half). Comparing both plots, we see that the increase of f/M lags at the via mouth

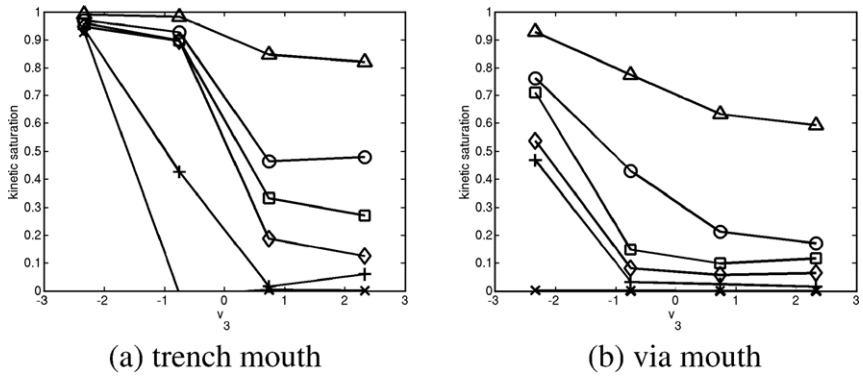

Fig. 6. Line plots of the saturation of the kinetic density $f(\mathbf{x}, \mathbf{v}, t)/M(\mathbf{v})$ for $Kn=1.0$ for $v_1=v_2=0$ as a function of v_3; (a) at the mouth of the trench at position $\mathbf{x}=(0.5, 0.5, 0.0)$ and (b) at the mouth of the via at position $\mathbf{x}=(0.5, 0.5, -0.3)$; at times: $\mathbf{x}=1$ ns, $+=2$ ns, $\diamond=3$ ns, $\square=4$ ns, $\circ=5$ ns, $\Delta=10$ ns.

deeper inside the feature than the trench mouth. More extensive studies of flow in this domain are shown in [21].

5. Discussion and conclusions

The results demonstrate that lower *Kn* lead to longer transients, as seen by lower species concentrations *c* deeper inside the features at each time. When transients on this time scale are considered, access to the kinetic density $f(\mathbf{x}, \mathbf{v}, t)$ as a function of $\mathbf{v}$ allows us to analyze the dependence of *f* on velocity components. For example, inside the features there are no reactant gas molecules traveling upwards during the initial transient. The *f* values for upward velocities increase as a result of re-emission of molecules that did not react on the wafer surface. This is particularly notable for larger *Kn* values. For simulations with very low *Kn*, we see that *f* is smaller for all velocities for a given time. It is this latter effect that leads to the longer transients. We can also observe that the shape of *f* approaches that of a Maxwellian faster for very low *Kn* and thus macroscopic observables such as the concentration c represent the transients adequately. This means that the added computational effort required to simulate a kinetic model may not be warranted in these cases, and traditional methods for continuum models may provide all of the details needed. But for models with moderate to large *Kn*, insight into the behavior of the model at small times is gained from the kinetic density, and so the effort of determining *f* may be useful in these cases.

These observations agree heuristically with the notion that the downward direction of the flow to the gas-solid interface is unimpeded for free molecular flow ($Kn=\infty$), and more molecules reach the feature bottom faster than for the collisional flows at lower *Kn*. If transients are important to understanding a given process, it is important to develop and test a simulator for the range of *Kn* of potential interest, before using it in the context of multiscale models. Specifically, it is apparent that intermediate scale models, for which $0.1 \le Kn \le 10.0$ might hold, will in fact motivate the use of kinetic solvers.

Acknowledgments

The hardware used in the computational studies was partially supported by the SCREMS grant DMS-0215373 from the U.S. National Science Foundation with additional support from the University of Maryland, Baltimore County. See www.math.umbc.edu/~gobbert/ kali for more information on the machine and the projects using it. Prof. Cale acknowledges support from MARCO, DARPA, and NYSTAR through the Interconnect Focus Center.

References

[1] A. Kersch, W.J. Morokoff, Transport Simulation in Microelectronics, vol. 3, Progress in Numerical Simulation for Microelectronics, Birkhäuser Verlag, Basel, 1995.
[2] C.R. Kleijn, C. Werner, Modeling of Chemical Vapor Deposition of Tungsten Films, vol. 2, Progress in Numerical Simulation for Microelectronics, Birkhäuser Verlag, Basel, 1993.
[3] T.S. Cale, T.P. Merchant, L.J. Borucki, A.H. Labun, Thin Solid Films 365 (2000) 152.
[4] T.S. Cale, G.B. Raupp, T.H. Gandy, J. Vac. Sci. Technol. A 10 (1992) 1128.
[5] C. Cercignani, The Boltzmann Equation and Its Applications, vol. 67, Applied Mathematical Sciences, Springer-Verlag, 1988.
[6] C. Cercignani, Cambridge Texts in Applied Mathematics, Cambridge University Press, 2000.
[7] A. Hasper, J. Holleman, J. Middelhoek, C.R. Kleijn, C.J. Hoogendoorn, J. Electrochem. Soc. 138 (1991) 1728.
[8] T.S. Cale, J.-H. Park, T.H. Gandy, G.B. Raupp, M.K. Jain, Chem. Eng. Commun. 119 (1993) 197.
[9] M.K. Gobbert, C.A. Ringhofer, T.S. Cale, J. Electrochem. Soc. 143 (1996) 2624.
[10] M.K. Gobbert, T.P. Merchant, L.J. Borucki, T.S. Cale, J. Electrochem. Soc. 144 (1997) 3945.
[11] T.P. Merchant, M.K. Gobbert, T.S. Cale, L.J. Borucki, Thin Solid Films 365 (2000) 368.
[12] FIDAP 7.6, Fluid Dynamics International, 500 Davis St., Ste. 600, Evanston, IL 60201, 1996.
[13] EVOLVE is a low pressure transport and reaction simulator developed by Timothy S. Cale with funding from the Semiconductor Research Corporation, the National Science Foundation, and Motorola.
[14] M.K. Gobbert, S.G. Webster, T.S. Cale, J. Electrochem. Soc. 149 (2002) G461.
[15] M.K. Gobbert, V. Prasad, T.S. Cale, J. Vac. Sci. Technol. B 20 (2002) 1031.
[16] M.K. Gobbert, V. Prasad, T.S. Cale, Thin Solid Films 410 (2002) 129.
[17] V. Prasad, M.K. Gobbert, M. Bloomfield, T.S. Cale, in: B.M. Melnick, T.S. Cale, S. Zaima, T. Ohta (Eds.), Advanced Metallization Conference 2002, Materials Research Society, 2003, p. 709.
[18] M.K. Gobbert, T.S. Cale, J. Comput. Phys. 213 (2006) 591.
[19] M.K. Gobbert, S.G. Webster, T.S. Cale, J. Sci. Comput. 30 (2007) 237.
[20] M.K. Gobbert, M.L. Breitenbach, T.S. Cale, in: V.S. Sunderam, G.D. van Albada, P.M.A. Sloot, J.J. Dongarra (Eds.), Computational Science—ICCS 2005, Lecture Notes in Computer Science, vol. 3516, Springer-Verlag, 2005, p. 41.
[21] M.K. Gobbert, T.S. Cale, Int. J. Multiscale Comput. Eng. 4 (2006) 319.
[22] J.-F. Remacle, J.E. Flaherty, M.S. Shephard, SIAM Rev. 45 (2003) 53.